



**HAL**  
open science

## Rapid and Wash-Free Time-Gated FRET Histamine Assays Using Antibodies and Aptamers

Hui-Jun Fu, Ruifang Su, Lin Luo, Zi-Jian Chen, Thomas Just Sørensen, Niko Hildebrandt, Zhen-Lin Xu

► **To cite this version:**

Hui-Jun Fu, Ruifang Su, Lin Luo, Zi-Jian Chen, Thomas Just Sørensen, et al.. Rapid and Wash-Free Time-Gated FRET Histamine Assays Using Antibodies and Aptamers. ACS sensors, 2022, pp.acssensors.2c00085. 10.1021/acssensors.2c00085 . hal-03624250

**HAL Id: hal-03624250**

**<https://normandie-univ.hal.science/hal-03624250>**

Submitted on 26 Jan 2023

**HAL** is a multi-disciplinary open access archive for the deposit and dissemination of scientific research documents, whether they are published or not. The documents may come from teaching and research institutions in France or abroad, or from public or private research centers.

L'archive ouverte pluridisciplinaire **HAL**, est destinée au dépôt et à la diffusion de documents scientifiques de niveau recherche, publiés ou non, émanant des établissements d'enseignement et de recherche français ou étrangers, des laboratoires publics ou privés.

# Rapid and wash-free time-gated FRET histamine assays using antibodies and aptamers

Hui-Jun Fu,<sup>a,b</sup> Ruifang Su,<sup>a,c</sup> Lin Luo,<sup>b</sup> Zi-Jian Chen,<sup>b</sup> Thomas Just Sørensen,<sup>c</sup>

Niko Hildebrandt,<sup>\*a,d,e</sup> Zhen-Lin Xu<sup>\*b</sup>

<sup>a</sup> nanoFRET.com, Laboratoire COBRA (Chimie Organique, Bioorganique, Réactivité et Analyse - UMR6014 & FR3038), Université de Rouen Normandie, CNRS, INSA, Normandie Université, 76000 Rouen, France.

<sup>b</sup> Guangdong Provincial Key Laboratory of Food Quality and Safety/ Guangdong Laboratory of Lingnan Modern Agriculture, South China Agricultural University, Guangzhou 510642, China.

<sup>c</sup> Nano-Science Center & Department of Chemistry, University of Copenhagen, Universitetsparken 5, 2100 Copenhagen, Denmark.

<sup>d</sup> Department of Chemistry, Seoul National University, Seoul 08826, South Korea.

<sup>e</sup> Université Paris-Saclay, 91405 Orsay Cedex, France.

\* Corresponding authors: [niko.hildebrandt@univ-rouen.fr](mailto:niko.hildebrandt@univ-rouen.fr), [jallent@163.com](mailto:jallent@163.com)

E-mail addresses of all co-authors: [huijun\\_foo@163.com](mailto:huijun_foo@163.com) (Hui-Jun Fu); [ruifang.su@univ-rouen.fr](mailto:ruifang.su@univ-rouen.fr) (Rui-fang Su); [lin.luo@scau.edu.cn](mailto:lin.luo@scau.edu.cn) (Lin Luo); [guangdongchenzj@163.com](mailto:guangdongchenzj@163.com); (Zi-Jian Chen); [tjs@chem.ku.dk](mailto:tjs@chem.ku.dk) (Thomas Just Sørensen); [niko.hildebrandt@univ-rouen.fr](mailto:niko.hildebrandt@univ-rouen.fr) (Niko Hildebrandt); [jallent@163.com](mailto:jallent@163.com) (Zhen-Lin Xu)

**ABSTRACT:** Histamine (HA) is an indicator of food freshness and quality. However, high concentrations of HA can cause food poisoning. Simple, rapid, sensitive, and specific quantification can enable efficient screening of HA in food and beverages. However, conventional assays are complicated and time-consuming as they require multiple incubation, washing, and separation steps. Here, we demonstrate that time-gated Förster resonance energy transfer (TG-FRET) between terbium (Tb) complexes and organic dyes can be implemented in both immunosensors and aptasensors for simple HA quantification using a rapid, single-step, mix-and-measure assay format. Both biosensors could quantify HA at concentrations relevant in food poisoning with limits of detection of 0.19  $\mu\text{g/mL}$  and 0.03  $\mu\text{g/mL}$ , respectively. Excellent specificity was documented against the structurally similar food components tryptamine and L-histidine. Direct applicability of the TG-FRET assays was demonstrated by quantifying HA in spiked fish and wine samples with both excellent concentration recovery and agreement with conventional multistep enzyme-linked immunosorbent assays (ELISAs). Our results show that the simplicity and rapidity of TG-FRET assays do not compromise sensitivity, specificity, and reliability and both immunosensors and aptasensors have a strong potential for their implementation in advanced food safety screening.

**KEYWORDS:** *Aptasensors, Immunoassays, Food testing, Fluorescence, Förster resonance energy transfer*

Histamine (HA, molecular weight: 111.15 Da) is one of the most important biogenic amines that is involved in many human physiological processes.<sup>1,2</sup> It is also commonly found in food and beverages, such as seafood,<sup>3</sup> beer,<sup>4</sup> or wine,<sup>5</sup> but the low inherent concentrations do not cause any health hazard. However, when food is spoiled or rotten, high numbers of bacteria can result in the production of high levels of HA, which lead to food poisoning and allergic reactions. Typical toxicological symptoms of HA are similar to those of food allergies and include headache, nausea, sweating, itching, and hypotension.<sup>6-8</sup> Although the European Union, United States Food and Drug Administration (FDA), and China have set regulatory limits for HA in food ranging from 50 to 1000 mg/kg,<sup>9,10</sup> foodborne poisoning associated with HA ingestion has not been eradicated.<sup>11</sup> Thus, to ensure human health and evaluate the quality of food, simple and efficient monitoring of histamine in food and beverage samples is an important challenge for sensor development.

Histamine can be formed from L-histidine (essential amino acid) decarboxylation by microbial activity. Therefore, the specificity of the detection method is paramount. Historically, the major analytical approach for HA determination in food samples was chromatographic separation,<sup>12-16</sup> which is typically connected to high instrumentation costs and the necessity of trained operators. To meet the requirements for a more rapid and low-cost detection within a large number of samples, highly sensitive and specific immunological methods, such as enzyme-linked immunosorbent assays (ELISAs), using

specific HA antibodies have been used for HA sensing.<sup>17-22</sup> Aptamers are alternative molecular recognition elements, usually composed of deoxyribonucleic acid (DNA) or ribonucleic acid (RNA) oligonucleotides (typically 15-80 nucleotides) that can bind their target via the formation of specific three-dimensional structures in aqueous solution.<sup>23</sup> The specificity and affinity of aptamer-target binding can be equivalent or even stronger than for antibodies.<sup>24</sup> Despite the development of advanced antibodies and aptamers, most of these developed assays for HA analysis are heterogeneous, which means that they include several inevitable and time-consuming washing and separation steps.<sup>25,26</sup> Only few simple and rapid single-step (homogeneous) assays, such as aptamer-based assays using colorimetry (gold nanoparticle aggregation or dispersion)<sup>27</sup> and fluorescence (quenching or recovery),<sup>28</sup> have been developed but inevitably suffered from interferences with the sample environment.

Förster resonance energy transfer (FRET) is a strongly donor-acceptor distance-dependent energy transfer mechanism that has been widely used for the quantification of biomolecular distances and concentrations via fluorescence biosensing.<sup>29-32</sup> FRET-based immunoassays are usually sandwich assays (binding of donor-antibody and acceptor-antibody to the same target results in FRET) or competitive assays (free target competes with donor or acceptor labeled target that is bound to an acceptor or donor labeled antibody) and have the advantage of simpler and quicker wash-free procedures (the binding-related FRET signal is different from other non-specific signals) and more precise ratiometric

detection (if both donor and acceptor are fluorescent).<sup>30,32,33</sup> When lanthanide-based donors with very long (up to milliseconds) excited state lifetimes are used in FRET, the use of time-gated (TG) detection can efficiently reduce sample autofluorescence and other interfering signals, resulting in highly sensitive homogeneous assay formats.<sup>30,34–36</sup> Using terbium (Tb) donors and dye or quantum dot acceptors, we have developed non-competitive TG-FRET assays against various protein or nucleic acid biomarkers.<sup>35,37–41</sup> However, implementing TG-FRET into specific, sensitive, rapid, and wash-free competitive assays for small molecules, such as histamine, remains to be demonstrated. For an efficient translation into different sensing concepts, it would also be highly desirable, if such a homogeneous HA assay could be generically applied to different molecular recognition molecules, such as antibodies and aptamers. Moreover, direct applicability to actual food samples would be extremely important.

Here, we present the development and application of two different competitive homogeneous TG-FRET assays for rapid and simple HA quantification. The first assay is based on the competition between a Tb-donor conjugated antigen and HA, both binding to an antibody (immunoglobulin G, IgG) labeled with dye-acceptors. We show that different dyes can be used to tune the concentration range and sensitivity of the assay. The second assay uses the competition between Tb-cDNA-to-dye-aptamer hybridization and HA-to-aptamer binding. The performance of the two assay formats was compared. Both assays showed excellent HA sensing performance and allowed us to perform HA concentration

recovery experiments in spiked fish and wine samples. We also performed a comparison to conventional heterogeneous ELISA, which showed that both TG-FRET assays could simply and rapidly quantify HA with high accuracy and reliability in actual food and beverage samples. With these advantages, the homogeneous TG-FRET assays have a strong potential for their implementation into rapid food and beverage quality monitoring.

## **MATERIALS AND METHODS**

**Materials.** Lumi4-Tb-NHS (Tb-NHS) complexes were provided by Lumiphore, Inc. (Berkeley, USA) Cyanine5.5 NHS ester (Cya5.5-NHS) and sulfo-Cyanine5.5-NHS ester (sulfoCya5.5-NHS) were purchased from Lumiprobe GmbH (Hannover, Germany). ATTO-655-NHS was purchased from ATTO-TEC GmbH (Siegen, Germany). Cy5.5 (GE Healthcare) was purchased readily conjugated to the RNA aptamer from Eurogentec (Seraing, Belgium). Chemical structures of these FRET donors and acceptors can be found in **Supporting Figure S1**. Anti-HA monoclonal antibody and antigen (specific hapten with ovalbumin, OVA, as carrier protein) were produced by our lab as previously reported.<sup>22</sup> HA was purchased from Heowns Biochem Technologies Co. Ltd. (Tianjin, China). The analogues of HA (such as L-histidine and tryptamine), Tris base, phosphate buffered saline (PBS), hydrochloric acid (HCl), sodium hydroxide (NaOH), N,N-dimethylformamide (DMF), sodium bicarbonate (NaHCO<sub>3</sub>), 4-(2-hydroxyethyl) piperazine-1-ethanesulfonic acid (HEPES), and bovine serum albumin (BSA) were purchased at Merck/Sigma-Aldrich

(St. Quentin Fallavier, France). Cy5.5 conjugated aptamers and complementary chain were synthesized and purified by high-performance liquid chromatography (HPLC) from Eurogentec. Their sequences are shown in **Table 1**. Gel electrophoresis (**Supporting Figure S2**) showed only one band between 25 to 50 bp, which confirmed that the aptamer (37 nt) did not form multiple secondary structures under the reaction condition and can be efficiently used for HA binding. High-quality Milli-Q water (18.2 MΩ.cm) was used for preparing solutions.

**Table 1.** Sequences of aptamer and complementary chain.

Name	Sequence (5'→3') <sup>a</sup>
Aptamer (RNA) <sup>b,c</sup>	Cy5.5-5'- <u><b>UACGAUCCAGUGG</b></u> GUUGAAGGAAAGUAACAGAUCGUA-3'
Complementary chain (DNA)	NH <sub>2</sub> -C6--5'- <u><b>CCACTGGATCGTA</b></u> -3'

<sup>a</sup> Complementary parts show in bold and underlined. <sup>b</sup> Because the aptamer is RNA, it contains uracil (U) instead of thymine (T). <sup>c</sup> The Cy5.5 dye conjugated to the aptamer is a different dye (Cy5.5 - GE Healthcare) than the Cya5.5 dye (Cyanine5.5 - Lumiprobe) conjugated to antibodies.

**Optical Spectroscopy.** Ultraviolet-visible (UV-vis) absorption spectroscopy was carried out on a Cary 60 UV-Vis spectrophotometer (Agilent, Santa Clara, USA). The photoluminescence (PL) emission spectrum of Tb was recorded on FluoTime 300 fluorescence spectrometer (PicoQuant, Berlin, Germany). PL emission spectra of the dyes were recorded on a Xenius XM fluorometer (SAFAS, Monaco). Because the quantum efficiency of the photon detector is very low beyond ~775 nm (which results in an overcorrection of the spectra beyond 775 nm), we recorded PL emission spectra until 775 nm only. TG-FRET assays were performed on a KRYPTOR compact PLUS fluorescence

plate reader (Cezanne/BRAHMS/Thermo Fisher Scientific, Nîmes, France) with a time gate between 0.1 and 0.9 ms after pulsed excitation at 337.1 nm using an integrated nitrogen laser operating at 20 Hz with 100 pulses. The time delay of 0.1 ms, detection window time of 0.8 ms, and excitation with 100 pulses were selected to efficiently suppress all short-lifetime background (e.g., sample autofluorescence) and to collect a sufficient amount of photons within a relatively short measurement time (100 pulses at 20 Hz corresponds to 5s). These parameters were based on our long-term experience with TG-FRET assays but in principle, also other parameters can be used. PL decays were recorded on a fluorescence lifetime plate reader (Edinburgh Instruments, Edinburgh, UK). Optical transmission bandpass filter (Semrock, Rochester, USA) wavelengths were  $494\pm 10$  nm for the Tb donor detection channel and  $716\pm 20$  nm for dye acceptor detection channel (Cy5.5, SulfoCy5.5, ATTO 655).

**Bioconjugation.** The complete antigen (hapten-labeled OVA carrier protein) was used for Tb-NHS bioconjugation because OVA provided accessible amino groups, which was not the case for the hapten. In addition, direct attachment of Tb to the hapten may interfere with antibody binding. 8 nM Lumi4-Tb-NHS was dissolved in DMF and then mixed with the antigen in 100  $\mu$ L of 100 mM carbonate buffer (pH 9.0) using a 30:1 (330  $\mu$ M Tb and 11  $\mu$ M antigen) reaction ratio. The mixture was incubated for 4 h at 25 rpm (rotations per minute) at room temperature using an ELMi Intelli-Mixer (Riga, Latvia). For purification, the sample was washed 4 times with 100 mM Tris-HCl (pH 7.4) using Zeba Spin desalting

columns (Thermo Fisher Scientific, France) with 7K molecular weight cut-off (MWCO). For Tb-complementary chain conjugates, 20-fold molar excess of Tb-NHS was mixed with the amino-functionalized complementary oligo (200  $\mu\text{M}$  Tb and 10  $\mu\text{M}$  DNA) and incubated in 100  $\mu\text{L}$  of 100 mM carbonate buffer (pH 9.0) overnight at 4  $^{\circ}\text{C}$ . The conjugates were purified 3 times with HEPES buffer (100 mM, pH 7.4) using Zeba Spin desalting columns with 7K MWCO. Tb concentrations were determined by absorbance measurements at 340 nm using an extinction coefficient of 26,000  $\text{M}^{-1} \text{cm}^{-1}$ . Antigens were quantified by absorbance measurements at 280 nm using an extinction coefficient of 31,400  $\text{M}^{-1} \text{cm}^{-1}$  (OVA). The oligo concentration was obtained by measuring the absorbance at 260 nm using an extinction coefficient of 124,800  $\text{M}^{-1} \text{cm}^{-1}$ .

For preparation of dye-IgG conjugates, Cya5.5-NHS, ATTO655-NHS, or sulfoCya5.5-NHS were mixed with IgG in 50  $\mu\text{L}$  of 100 mM carbonate buffer (pH 8.0) using a 8:1 (208  $\mu\text{M}$  dye and 26  $\mu\text{M}$  IgG) reaction ratio and incubated for 4h at 25 rpm at room temperature using an ELMI Intelli-Mixer. After the same purification procedure as for Tb conjugation, the conjugation ratios were determined by absorption spectroscopy, using linear combinations of the IgG and dye absorption spectra to best fit the absorption spectra of the IgG-dye conjugates. IgG concentration was determined using an extinction coefficient of 210,000  $\text{M}^{-1} \text{cm}^{-1}$  at 280 nm. Because the dye absorption spectra significantly changed upon IgG conjugation, the original dye spectra (using the peak extinction coefficients provided by the suppliers: 198,000  $\text{M}^{-1} \text{cm}^{-1}$  for Cya5.5; 235,000  $\text{M}^{-1} \text{cm}^{-1}$  for

SulfoCya5.5;  $125,000 \text{ M}^{-1} \text{ cm}^{-1}$  for ATTO655) were corrected, such that the integrals of the original (dye in buffer) and changed (IgG-conjugated dye) spectra were the same (**Supporting Figure S3**). These corrected extinction coefficient spectra were used for calculating the dye concentrations in the IgG-dye conjugates.

**Determination of FRET Parameters.**<sup>42</sup> Förster distances ( $R_0$ , donor-acceptor distance for which FRET efficiency is 50%) were calculated using the following equations:

$$R_0 = 0.021 (\kappa^2 \Phi_D n^{-4} J)^{1/6} \text{ nm} \quad (1)$$

$$J = \int_{475\text{nm}}^{700\text{nm}} I_D(\lambda) \epsilon_A(\lambda) \lambda^4 d\lambda \quad (2)$$

A dipole-dipole orientation factor ( $\kappa^2$ ) of 2/3 was assumed, as justified by the random orientation of donor and acceptor during the FRET time (dynamic averaging) taking into account the long PL lifetime of the Tb donor and their unpolarized emission. The Tb-centered PL quantum yield ( $\Phi_D$ ) was  $0.7 \pm 0.1$ . For aqueous solutions, the refractive index of the medium ( $n$ ) was taken as 1.35. The overlap integral ( $J$ ) was calculated by the spectral overlap between the area normalized (to unity) PL spectrum of Tb (the entire spectrum between 475 and 700 nm)<sup>43</sup> and the molar extinction coefficient ( $\text{M}^{-1} \text{cm}^{-1}$ ) spectrum of the dyes from 475 to 700 nm (cf. **Figure 1A**).

**Procedures for TG-FRET assays.** Two different homogeneous TG-FRET assays based on IgG and aptamer recognition of HA were developed. In the IgG system, all samples were prepared in 100 mM Tris-HCl containing 0.5% (w/w) BSA buffer. Measurement mixtures (150  $\mu\text{L}$ ) were composed of 50  $\mu\text{L}$  IgG-dye, 50  $\mu\text{L}$  antigen-Tb, and

50  $\mu\text{L}$  HA solutions at different concentrations and incubated at room temperature for 2 h. For the aptamer system, all samples were prepared in HEPES buffer (50 mM HEPES, pH 7.0, 250 mM NaCl, and 0.1 mM  $\text{MgCl}_2$ , 0.01% Tween 20). Measurement mixtures (150  $\mu\text{L}$ ) were composed of 50  $\mu\text{L}$  of Tb-cDNA, 50  $\mu\text{L}$  of dye-aptamer, and 50  $\mu\text{L}$  of HA, heated to 55°C for 20 min, and then incubated at 22°C for 1h. TG-FRET assay and PL decay measurements (performed in black 96-well KRYPTOR microplates - Thermo Fisher Scientific) were performed using 140  $\mu\text{L}$  of the measurement mixtures. TG-FRET assays take 5 s per sample (100 pulses with a repetition rate of 20 Hz). Both IgG and aptamer based assays are single-step assays (no separation or washing steps) that only require a certain incubation time. The total assay times were 120 min for the IgG-based assays and 80 min for the aptamer-based assays.

Assay calibration curves were recorded as the relative FRET ratio (Equation 3) against HA concentration. FRET ratios (Equation 4) were calculated from the TG intensities (0.1-0.9 ms) in the acceptor ( $I^A$ ) and donor ( $I^D$ ) detection channels and FRET ratio ( $c=0$ ) presents the FRET ratio of samples without HA (zero analyte control), whereas FRET ratio ( $c=x$ ) presents the FRET ratio of samples with a specific concentration ( $x$ ) of HA. All samples were measured in triplicate. In cases where error bars are invisible, they were smaller than the data points.

$$\text{rel. FRET ratio} = \frac{\text{FRET ratio } (c=x)}{\text{FRET ratio } (c=0)} \quad (3)$$

$$\text{FRET ratio} = \frac{I^A}{I^D} \quad (4)$$

**Preparation of Food Samples.** It has been reported that certain seafood is rich in free histidine in the muscle, which can be transformed into HA and lead to HA contamination.<sup>44,45</sup> In addition, fermented food or beverages, such as wine, can also contain high HA concentrations due to microbial activity.<sup>46,47</sup> Considering this, we purchased fresh salmon and wine (both supposed to have negligible HA concentrations) from a local supermarket as representative samples to assess the practicality of the developed TG-FRET immunoassays. Samples were prepared as previously reported.<sup>22</sup> In brief, 2 g of salmon were mixed with 2 mL PBS and homogenized. 8 mL of PBS were added into the homogenate (2 g) and shaken vigorously for 1 min. The mixture was centrifuged at 3000 g for 10 min and the water layer of supernatant was diluted 20-fold in PBS. This solution was then spiked with different concentrations of HA standard, namely 100, 200, and 400 mg per kg of fresh fish for TG-FRET assays and conventional ELISAs. For wine, 1 mL of wine was added into 9 mL PBS and then spiked with different concentrations of HA standard, namely 10, 15, and 20 mg per L of wine, for TG-FRET assays and conventional ELISAs. Methods for isothermal titration calorimetry (ITC), nucleic acid electrophoresis, and ELISA assays are reported in the Supporting Information.

## RESULTS AND DISCUSSION

**Characterization of the FRET systems.** Acceptor dyes were selected, such that their absorption would significantly overlap with the Tb donor emission and that their PL could be measured beyond the Tb emission spectra (wavelengths larger than 700 nm). In principle, also other lanthanide complexes or nanoparticles (containing trivalent ions of, e.g., Eu, Sm, Dy, or Er) emitting in the visible spectrum could be selected as appropriate donors.<sup>36</sup> However, combining Tb donors with very red (emission beyond 700 nm) dye acceptors was shown to result in very low Tb background PL and strong dye-sensitization.<sup>41</sup> The selection criteria also allowed us to compare different types of organic fluorophores and the variations in the bioconjugates. Four similar dyes Cyanine5.5 (Cya5.5), Sulfo-Cyanine5.5 (sulfoCya5.5), ATTO 655 (ATTO655), and Cy5.5 were used in the Tb-dye donor-acceptor pairs. As shown in **Figure 1A**, the area-normalized Tb emission spectra (gray) and absorption spectra of the different dye acceptors exhibited good spectral overlap, which resulted in similar overlap integrals (from 475 nm to 700 nm) of  $J(\text{Tb-Cya5.5}) = 2.4 \times 10^{15} \text{ M}^{-1}\text{cm}^{-1}\text{nm}^4$ ,  $J(\text{Tb-sulfoCya5.5}) = 3.4 \times 10^{15} \text{ M}^{-1}\text{cm}^{-1}\text{nm}^4$ ,  $J(\text{Tb-ATTO655}) = 2.7 \times 10^{15} \text{ M}^{-1}\text{cm}^{-1}\text{nm}^4$ , and  $J(\text{Tb-Cy5.5}) = 3.4 \times 10^{15} \text{ M}^{-1}\text{cm}^{-1}\text{nm}^4$  and Förster distances of  $R_0(\text{Tb-Cya5.5}) = 5.5 \pm 0.4 \text{ nm}$ ,  $R_0(\text{Tb-sulfoCya5.5}) = 5.9 \pm 0.4 \text{ nm}$ ,  $R_0(\text{Tb-ATTO655}) = 5.7 \pm 0.4 \text{ nm}$ , and  $R_0(\text{Tb-Cy5.5}) = 5.9 \pm 0.2 \text{ nm}$ . The different shapes of the dye absorption spectra resulted from the slightly different types of dyes as well as from the different bioconjugates (the dye spectra shown in **Figure 1** correspond to the IgG and

aptamer conjugated dyes - comparison with the dye spectra in solution are shown in **Supporting Figure S3**). These different dye-bioconjugate conditions led to different environments that caused non-specific adsorption or aggregation of some of the dyes, which, in turn, resulted in spectral broadening and redshift as well as an increase of the lower-wavelength absorption peak compared to the higher-wavelength peak.<sup>48–50</sup> This behavior is very well illustrated by the different Cya5.5 absorption spectra, for which sulfoCya5.5 (green spectrum in **Figure 1A**) shows less aggregation compared to Cya5.5 (magenta spectrum in **Figure 1A**). The emission spectra (**Figure 1B**) also show differences in the spectral positions of their peaks. However, all of them provided significant PL emission beyond 700 nm to avoid overlap with Tb PL. Ratiometric TG PL detection was performed in two detection channels, namely  $494\pm 10$  nm for Tb and  $716\pm 20$  nm for the dyes (bandpass filter transmission spectra are shown in gray in **Figure 1B**).

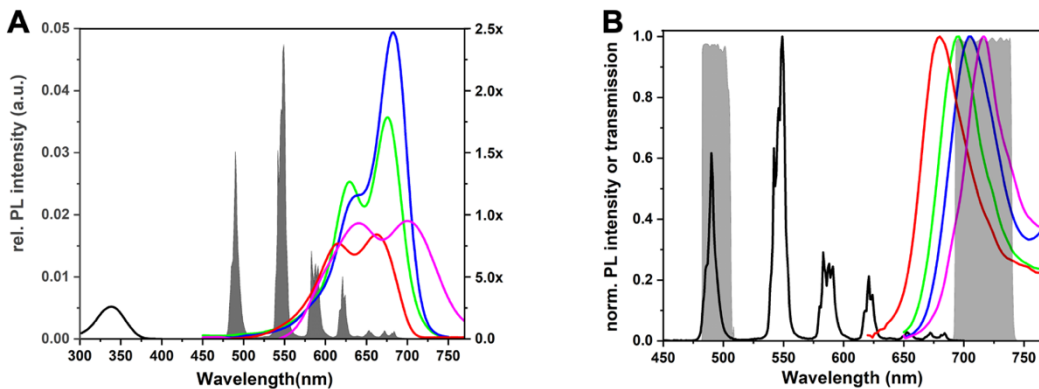


**Figure 1.** Absorption and emission spectra of the FRET donor and acceptors. **(A)** Absorption spectra of Tb (black), Cya5.5 (magenta), sulfoCya5.5 (green), ATTO655 (red), and Cy5.5 (blue). The area-normalized Tb emission spectrum (gray) is shown for visualization of donor-acceptor spectral overlap. **(B)** PL emission spectra of Tb (black), Cya5.5 (magenta), sulfoCya5.5 (green), ATTO655 (red), and Cy5.5 (blue). Excitation wavelengths were  $340\pm 2.5$  nm for Tb and  $630\pm 2.5$  nm for the dyes. Bandpass filter transmission spectra for Tb donor and dye acceptor detection channels

are shown in gray.

**TG-FRET immunosensor and aptasensor detection principles.** Although TG-FRET detection is the same for both assay types, the mechanisms of HA quantification using antibodies (**Figure 2A**) or aptamers (**Figure 2B**) are significantly different. The immunosensor is used in a competitive immunoassay, in which a Tb-labeled antigen and HA compete for binding sites on dye-labeled IgGs. The aptasensor, which is composed of a dye-labeled aptamer and a Tb-labeled complementary DNA (cDNA), is separated via the specific HA-aptamer interaction, which displaces the cDNA from the aptamer. Both competitive assays result in decreasing FRET (less FRET pairs) with increasing HA concentration because FRET is disrupted via HA-IgG and HA-aptamer binding. Both TG-FRET assays were ratiometric, which means that TG dye acceptor and donor PL intensities were measured simultaneously and their ratio (rel. FRET ratio, Equation 3) was used for HA quantification.

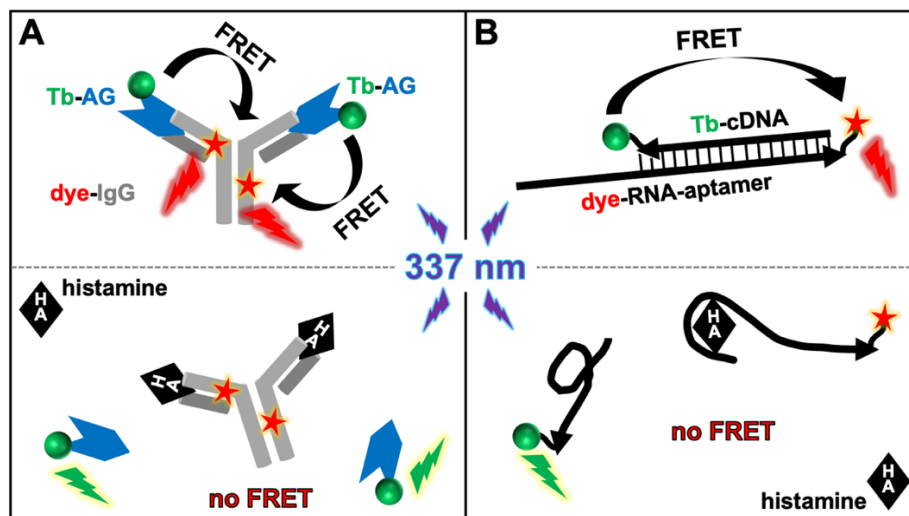


**Figure 2.** TG-FRET assay principles based on competition of Tb-antigen (Tb-AG) and HA for dye-

IgG binding (**A**) or competition between Tb-cDNA/dye-aptamer hybridization and HA-aptamer binding (**B**).

### **Influence of the type of dye-IgG bioconjugate on immunosensor**

**performance.** TG-FRET immunoassays were used to investigate the influence of the specific nature of the antibody-dye conjugate on the assay performance. All dyes were labeled (using the same conditions) via their functional NHS ester groups to free amines on the anti-HA IgG. Bioconjugation of the dyes to the IgG resulted in partial dye adsorption and aggregation as witnessed by the redshifted and broadened absorption spectra (vide supra). SulfoCya5.5 was least affected by IgG-conjugation (no broadening and higher intensity ratio of long-wavelength to short-wavelength absorption peaks - cf. **Figure 1A**), which indicated that the negatively charged sulfo groups provided a better solubility of the IgG-conjugated dye (and therefore less adsorption and aggregation) in the carbonate buffer used for bioconjugation. Despite the differences, all three IgG-dye conjugates were functional. A comparative assay (**Supporting Figure S4** and **Table 2**), performed at the same IgG concentrations (12.4 nM), antigen concentrations (27.4 nM), and HA concentration range (0 - 400 µg/mL), showed that assays with SulfoCya5.5-IgG had a significantly broader detection and concentration range. On the other hand, Cya5.5-IgG provided a lower limit of detection (LOD), which may be related to the lower amount of dyes per IgG or the better overlap of the PL emission with the wavelength range of the detection filter (cf. **Figure 2B**). Although a more detailed bioconjugation study would be

necessary to understand how the different dyes can be used to adjust the assay performance, the different types of dyes clearly resulted in different assay calibration curves, which showed that the choice of acceptor dye and bioconjugation procedure plays an important role in TG-FRET sensor development. In the case of HA quantification, where relatively high concentrations need to be distinguished, the SulfoCya5.5-IgG conjugates with the broadest detection and concentration range are most probably the best choice.

**Table 2.** Comparison of assay performance using different IgG-dye conjugates.

Dye	Conjugation ratio (dye/IgG)	Detection range <sup>a</sup>	Linear range ( $\mu\text{g}/\text{mL}$ ) <sup>b</sup>	IC <sub>50</sub> in $\mu\text{g}/\text{mL}$	LOD (IC <sub>10</sub> ) in $\mu\text{g}/\text{mL}$
Cya5.5	2.4 $\pm$ 1.2	~0.4	0.10 - 1.97	0.45 $\pm$ 0.05	0.040 $\pm$ 0.005
ATTO655	4.9 $\pm$ 2.0	~0.5	0.39 - 5.87	1.52 $\pm$ 0.18	0.18 $\pm$ 0.03
SulfoCya5.5	3.2 $\pm$ 1.0	~0.8	0.53 - 18.2	3.11 $\pm$ 0.36	0.19 $\pm$ 0.03

<sup>a</sup> Difference between the highest and lowest relative FRET-ratios in the calibration curves. <sup>b</sup> Both minimum and maximum values have 20% relative errors.

**Comparison of TG-FRET HA immunosensors and aptasensors.** Bioconjugation of the RNA aptamer and c-DNA was quite different from the random labeling of IgG with several dyes because the nucleic acids were functionalized only on their two termini (3' and/or 5'). Normally, this results in significantly less adsorption or aggregation issues and makes donor-acceptor distance control much easier. However, the 1:1 donor-acceptor ratio can also result in less overall FRET signal changes upon target binding, thus, leading to a higher background signal at high target concentrations. This assumption was confirmed by a direct comparison of the HA assays in a 0.03 to 400  $\mu\text{g}/\text{mL}$  concentration range using

both immunosensors (SulfoCya5.5-IgG with  $3.2 \pm 1.0$  dyes plus Tb-antigen with  $1.6 \pm 0.3$  Tb) and aptasensors (Cy5.5-aptamer with 1 dye and Tb-cDNA with 1 Tb). Both homogeneous TG-FRET assays showed excellent analytical performance over the entire concentration range (**Figure 3**). The signal change of both TG Tb PL increase and TG dye PL intensity decrease (and therefore also the rel. FRET ratio decrease) over the complete concentration range was significantly stronger for the IgG-based assay, thereby providing a larger detection range and better distinction of higher HA concentrations. At lower concentrations, the aptamer-based assay provided a better FRET ratio distinction and thus, also a lower LOD. To verify if this lower LOD was not caused by differences in HA binding affinity, we determined the dissociation constant of the IgG by isothermal titration calorimetry (ITC) and found a value of  $K_D = 0.53 \mu\text{M}$  (**Supporting Figure S8**), which was very close to the value reported for the RNA aptamer used in our study ( $0.4 \mu\text{M}$ ).<sup>24</sup> Therefore, we assume that the larger size of the antibody-antigen complex, composed of IgG ( $\sim 150$  kDa and  $6 \text{ nm} \times 9.5 \text{ nm} \times 15 \text{ nm}$  size)<sup>51</sup> and OVA ( $45$  kDa,  $7 \text{ nm} \times 4.5 \text{ nm} \times 5 \text{ nm}$ ),<sup>52</sup> requires higher HA concentrations for a significant change in FRET ratio compared to the relatively small aptamer-cDNA complex with a donor-acceptor distance of 13 base pairs, for which already low HA concentrations could result in significant FRET changes. The PL intensities of the PL decay curves (**Figure 3**) were quite weak (due to the relatively low IgG and aptamer concentrations in the assays) and did not allow for a reliable PL lifetime analysis, which could have been used for measuring the donor-acceptor distances via the FRET

spectroscopic ruler.<sup>53,54</sup> However, the shapes of the PL decay curves clearly show a multiexponential decay for the IgG-based assays, which confirmed the donor-acceptor distance distribution caused by the multiple and randomly labeled dyes per IgG. The almost monoexponential decay for the aptamer-based assays confirmed the single donor-acceptor pair within the relatively rigid double stranded DNA-RNA hybrid.

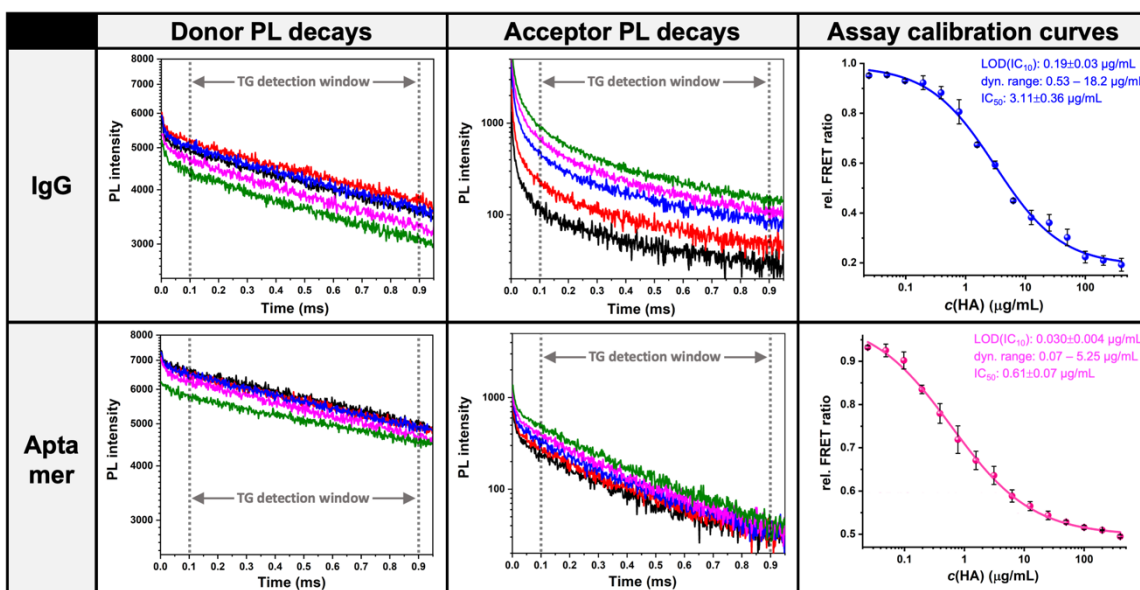


**Figure 3.** Selected PL decay curves of Tb donors and dye acceptors (green: no HA; magenta: 0.39 µg/mL HA; blue: 3.13 µg/mL HA; red: 25 µg/mL HA; black: 400 µg/mL HA) and HA assay calibration curves (showing all measured HA concentrations) of TG-FRET assays based on IgGs and aptamers. Dynamic range minimum and maximum values have an error of 20%. Determination of  $IC_{50}$  and  $IC_{10}$  values is shown in **Supporting Figure 5**. Donor and acceptor PL decay curves and TG PL intensities of all measured concentrations are shown in **Supporting Figures S6** (IgG assays) and **S7** (aptamer assays).

**Histamine selectivity of TG-FRET immunosensors and aptasensors.** In addition to good sensitivity (target-concentration dependent signal change) in a suitable target concentration range, the specificity of an assay is extremely important. This is

especially true when similar components can be found in the sample. In order to evaluate the specificity of both TG-FRET assay for HA, we used tryptamine, as a representative biogenic amine, and histidine, as precursor of histamine, as possibly interfering components. In particular, L-histidine exists at high concentration levels in related foods and its structure is closely related to the one of HA. Using the same conditions for HA, tryptamine, and L-histidine analysis, we found negligible cross-reactivity to L-histidine, and tryptamine (**Figure 4**), which demonstrated the excellent specificity of both IgG and aptamer based HA assays.

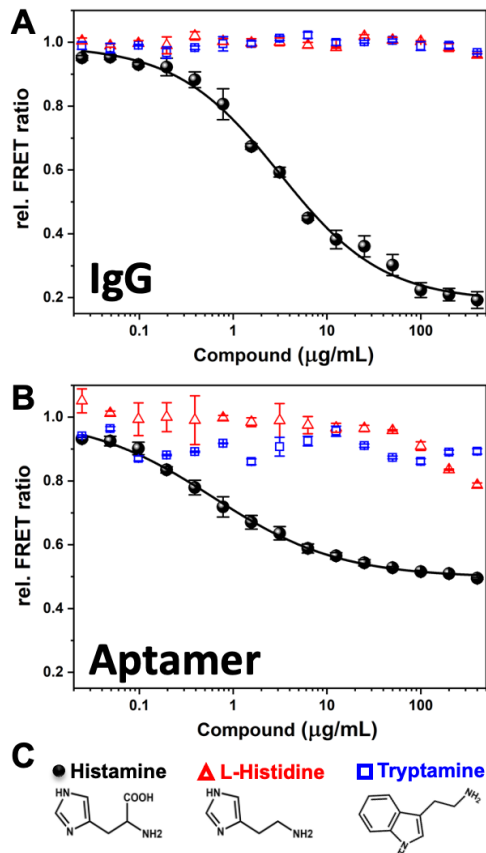


**Figure 4.** Specificity analysis of related analogues (L-histidine and tryptamine) of TG-FRET assays based on IgGs (**A**) and aptamers (**B**). Cross-reactivity ( $IC_{50}(\text{HA}) / IC_{50}(\text{cross-reactive compound})$ ) was below 0.1%. **C:** Chemical structures of the different compounds.

**Concentration recovery in spiked food samples.** Based on their favorable analytical performance and to go a significant step further toward actual food analysis, we challenged our homogeneous TG-FRET assays with HA spiking and concentration recovery experiments in fish and wine samples. Solutions extracted from fresh fish (200-fold diluted) and wine samples (10-fold diluted) were spiked with increasing levels of the HA standard (100, 200, and 400 mg per kg of fresh fish and 10, 15, and 20 mg per L of wine). The different samples were then analyzed by both TG-FRET assays and a conventional indirect competitive ELISA for comparison (calibration curves see **Figure S9**). As shown in **Figure 5**, all assays could very well quantify the HA concentrations. In the fish samples, IgG-based assays had a mean recovery rate of 103 to 107% and aptamer-based assays of 99 to 103%, with corresponding coefficients of variance (CVs) of 3 to 11% and 7 to 16%, respectively. In wine samples, recovery rates were 95 to 105% for IgG-based assays and 90 to 98% for the aptamer-based tests, with CVs of 6 to 11% and 3 to 12%, respectively. The excellent agreement with the results of the conventional heterogeneous ELISA assay clearly showed that the simplicity and rapidity of our homogeneous TG-FRET assays are combined with high accuracy and reproducibility. The recovery ranges were also in very good agreement to or better than for other IgG or aptamer based assays from previous studies (**Table 3**).

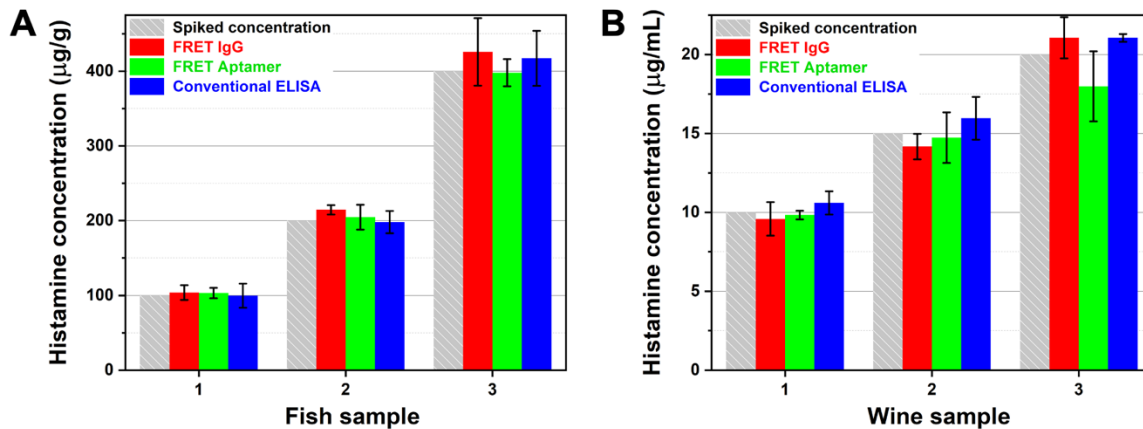


**Figure 5.** HA concentration recovery results in spiked fish (A) and wine (B) samples using TG-FRET-IgG assays (red), TG-FRET-aptamer assays (green), and conventional ELISA (blue). Gray columns present spiked concentrations. Full data is shown in **Supporting Table S1**.

**Table 3.** Mean recovery rates of different assays for HA analysis in fish and wine.

Recognition molecule	Assay format	Sample	Recovery	Reference	
IgG	heterogeneous	fish	83% - 95.7%	17	
		red wine	89.1% - 110.1%		
	homogeneous	fish	97.25% - 105%	18	
		saury	84.1% - 96%	22	
		red wine	92.5% - 106.8%		
		fish	98.28% - 98.68%	55	
		rice wine	91.52% - 91.58%		
		fish, prawn and crab	80.19% - 108.3%	20	
	Aptamer	homogeneous	fish	103.7% - 107.2%	this work
			red wine	94.5% - 105.3%	
fish			80% - 113%	24	
fish			86.34% - 123%	56	
		fish	99.5% - 103.1%	this work	
		red wine	89.9% - 98.3%		

## CONCLUSIONS

In conclusion, we successfully developed and tested two TG-FRET assays for simple and rapid HA quantification using IgGs or aptamers for HA binding. We first investigated the influence of different acceptor dyes on the immunoassay performance and found that sulfonated dyes provided a better solubility and less adsorption and aggregation when conjugated to IgG. Although the SulfoCya5.5-IgG immunosensors provided the broadest detection and concentration range, ATTO655-IgG and Cya5.5-IgG, which showed partial adsorption and aggregation when conjugated to IgG, were also functional in the HA assays, and the Cya5.5-IgG based assay even provided the lowest LOD of  $0.040\pm 0.005$   $\mu\text{g/mL}$ . Owing to the overall best performance, the SulfoCya5.5-IgG based assay with an LOD of  $0.19\pm 0.03$   $\mu\text{g/mL}$  was selected for comparison with the Cy5.5-aptamer based assay. The latter provided a less broad detection and concentration range but a lower LOD of  $0.030\pm 0.004$   $\mu\text{g/mL}$ , most probably due to the very different donor and acceptor conjugates. Various donors and acceptors in the IgG-antigen system resulted in a donor-acceptor distance distribution, whereas the single donor-acceptor pair in the aptamer-cDNA complex led to a well-defined donor-acceptor distance. Considering that both LODs were well below the regulatory limits for HA in food (50 to 1000 mg/kg), direct applicability to HA quantification in actual food samples was demonstrated by concentration recovery experiments in spiked fish and wine samples. The excellent recovery rates of TG-FRET were in very good agreement with results from conventional heterogeneous ELISA assays

but with a much simpler and faster assay format. Whereas the ELISA required *i)* overnight antigen incubation, *ii)* two washing steps, *iii)* blocking buffer incubation for 1h, *iv)* HA and IgG incubation for 40 min, *v)* five washing steps, *vi)* secondary antibody incubation for 40 min, *vii)* five washing steps, *viii)* TMB (tetramethylbenzidine) solution incubation for 10 min, and *ix)* H<sub>2</sub>SO<sub>4</sub> addition to stop the reaction, TG-FRET assays were performed in a single-step format by simply mixing all components, incubating for 120 min (IgG-based assays) or 80 min (aptamer-based assays), and measuring for 5 s. Taking into account the solution-phase format of TG-FRET assays, reduction of the incubation times should be possible to further reduce the overall assay time. In conclusion, our results showed that the important TG-FRET assay advantages of simplicity and rapidity go hand-in-hand with accuracy and reproducibility and that TG-FRET is suitability for the quantification of small contaminants in food with a strong potential for the development of rapid test kits for food and beverage analysis.

## **ASSOCIATED CONTENT**

### **Supporting Information**

Chemical structures of FRET donor and acceptors, gel electrophoresis analysis of aptamers, absorption spectra of pure and IgG-conjugated dyes, HA assay calibration curves for IgG assays with different dyes, PL decay curves and TG PL intensities of Tb donors and dye acceptors for IgG and aptamer based assays, IgG-HA affinity determination by ITC, ELISA

HA assay calibration curve, full data of concentration recovery results, and supporting methods.

### **Conflict of interest**

The authors declare no conflict of interest.

### **Acknowledgments**

We thank Lumiphore, Inc. for the gift of Lumi4 reagents. This work has been supported by China Scholarship Council (CSC), National Nature Science Foundation of China (31822039), National Research Foundation of Korea, Seoul National University, University of Copenhagen, Villum Fonden (grant#14922), Université Paris-Saclay, Université de Rouen Normandie, INSA Rouen, CNRS, Normandie Université, European Regional Development Fund, Labex SynOrg (ANR-11-LABX-0029), Carnot Institute I2C, XL-Chem graduate school (ANR-18-EURE-0020 XL CHEM), and Region Normandie.

### **REFERENCES**

- (1) Latorre-Moratalla, M. L.; Comas-Basté, O.; Bover-Cid, S.; Vidal-Carou, M. C. Tyramine and Histamine Risk Assessment Related to Consumption of Dry Fermented Sausages by the Spanish Population. *Food Chem. Toxicol.* **2017**, *99*, 78–85. <https://doi.org/10.1016/j.fct.2016.11.011>.
- (2) Gagic, M.; Jamroz, E.; Krizkova, S.; Milosavljevic, V.; Kopel, P.; Adam, V. Current Trends in Detection of Histamine in Food and Beverages. *J. Agric. Food Chem.* **2019**, *67* (3), 773–783. <https://doi.org/10.1021/acs.jafc.8b05515>.
- (3) Sivamaruthi, B. S.; Kesika, P.; Chaiyasut, C. A Narrative Review on Biogenic Amines in Fermented Fish and Meat Products. *J. Food Sci. Technol.* **2021**, *58* (5), 1623–1639. <https://doi.org/10.1007/s13197-020-04686-x>.

- (4) Cai, J.; Li, M.; Xiong, X.; Fang, X.; Xu, R. Detection of Histamine in Beer by Nano Extractive Electrospray Ionization Mass Spectrometry. *J. Mass Spectrom.* **2014**, *49* (1), 9–12. <https://doi.org/10.1002/jms.3315>.
- (5) Landete, J. m.; Ferrer, S.; Pardo, I. Which Lactic Acid Bacteria Are Responsible for Histamine Production in Wine? *J. Appl. Microbiol.* **2005**, *99* (3), 580–586. <https://doi.org/10.1111/j.1365-2672.2005.02633.x>.
- (6) El-Ghareeb, W. R.; Elhelaly, A. E.; Abdallah, K. M. E.; El-Sherbiny, H. M. M.; Darwish, W. S. Formation of Biogenic Amines in Fish: Dietary Intakes and Health Risk Assessment. *Food Sci. Nutr.* **2021**, *9* (6), 3123–3129. <https://doi.org/10.1002/fsn3.2271>.
- (7) Moniente, M.; García-Gonzalo, D.; Ontañón, I.; Pagán, R.; Botello-Morte, L. Histamine Accumulation in Dairy Products: Microbial Causes, Techniques for the Detection of Histamine-Producing Microbiota, and Potential Solutions. *Compr. Rev. Food Sci. Food Saf.* **2021**, *20* (2), 1481–1523. <https://doi.org/10.1111/1541-4337.12704>.
- (8) Perkins, R. A.; Morgan, S. S. Poisoning, Envenomation, and Trauma from Marine Creatures. *Am. Fam. Physician* **2004**, *69* (4), 885–890.
- (9) Wójcik, W.; Łukasiewicz, M.; Puppel, K. Biogenic Amines: Formation, Action and Toxicity – a Review. *J. Sci. Food Agric.* **2021**, *101* (7), 2634–2640. <https://doi.org/10.1002/jsfa.10928>.
- (10) Ruiz-Capillas, C.; Herrero, A. M. Impact of Biogenic Amines on Food Quality and Safety. *Foods* **2019**, *8* (2), 62. <https://doi.org/10.3390/foods8020062>.
- (11) Colombo, F. M.; Cattaneo, P.; Confalonieri, E.; Bernardi, C. Histamine Food Poisonings: A Systematic Review and Meta-Analysis. *Crit. Rev. Food Sci.* **2018**, *58* (7), 1131–1151. <https://doi.org/10.1080/10408398.2016.1242476>.
- (12) Zhang, X.; Hui, Y.; Jiang, M.; Cai, Y.; Huang, D.; Yang, G.; Kong, C. Determination of 6 Biogenic Amines in Food Using High-Performance Liquid Chromatography-Tandem Mass Spectrometry without Derivatization. *J. Chromatogr. A* **2021**, *1653*, 462415. <https://doi.org/10.1016/j.chroma.2021.462415>.
- (13) Kamankesh, M.; Mohammadi, A.; Ghanati, K. Determination of Biogenic Amines in Lighvan Cheese Using a Novel Hollow-Fibre Electromembrane-Microextraction Coupled with Gas Chromatography–Mass Spectrometry. *Int. J. Dairy Technol.* **2021**, *74* (4), 759–767. <https://doi.org/10.1111/1471-0307.12806>.
- (14) Chimalakonda, K. C.; Pang, E.; Weaver, J. L.; Howard, K. E.; Patel, V.; Boyne, M. T. Development and Validation of a Liquid-Chromatography Tandem Mass Spectrometry Method to Determine in Vitro and in Vivo Histamine Release. *Journal of Pharmaceutical and Biomedical Analysis* **2015**, *102*, 494–499. <https://doi.org/10.1016/j.jpba.2014.10.016>.
- (15) Chen, L.; Singh, V.; Rickert, D.; Khaled, A.; Pawliszyn, J. High Throughput Determination of Free Biogenic Monoamines and Their Metabolites in Urine Using Thin-Film Solid Phase Microextraction. *Talanta* **2021**, *232*, 122438. <https://doi.org/10.1016/j.talanta.2021.122438>.
- (16) Zhang, Y.; Yu, J.; Lai, S.; Song, J.; Wu, X.; Wang, D.; Pang, L.; Chai, T. Rapid Determination of Histamine Level in Seafood Using Read-out Strips Based on High-Performance Thin Layer

- Chromatography Modified with Self-Visualization Nanomaterials. *Food Control* **2021**, *122*, 107816. <https://doi.org/10.1016/j.foodcont.2020.107816>.
- (17) Luo, L.; Xu, Z.-L.; Yang, J.-Y.; Xiao, Z.-L.; Li, Y.-J.; Beier, R. C.; Sun, Y.-M.; Lei, H.-T.; Wang, H.; Shen, Y.-D. Synthesis of Novel Haptens and Development of an Enzyme-Linked Immunosorbent Assay for Quantification of Histamine in Foods. *J. Agric. Food Chem.* **2014**, *62* (51), 12299–12308. <https://doi.org/10.1021/jf504689x>.
- (18) Dong, X.-X.; Yang, J.-Y.; Luo, L.; Zhang, Y.-F.; Mao, C.; Sun, Y.-M.; Lei, H.-T.; Shen, Y.-D.; Beier, R. C.; Xu, Z.-L. Portable Amperometric Immunosensor for Histamine Detection Using Prussian Blue-Chitosan-Gold Nanoparticle Nanocomposite Films. *Biosens. Bioelectron.* **2017**, *98*, 305–309. <https://doi.org/10.1016/j.bios.2017.07.014>.
- (19) Mattsson, L.; Jungmann, C.; Lieberzeit, P. A.; Preininger, C. Modified Carbon Black as Label in a Colorimetric On-Chip Immunoassay for Histamine. *Sens. Actuators B Chem.* **2017**, *246*, 1092–1099. <https://doi.org/10.1016/j.snb.2016.11.141>.
- (20) Yang, F.; Xu, L.; Dias, A. C. P.; Zhang, X. A Sensitive Sandwich ELISA Using a Modified Biotin-Streptavidin Amplified System for Histamine Detection in Fish, Prawn and Crab. *Food Chem.* **2021**, *350*, 129196. <https://doi.org/10.1016/j.foodchem.2021.129196>.
- (21) Li, Y.-F.; Lin, Z.-Z.; Hong, C.-Y.; Huang, Z.-Y. Histamine Detection in Fish Samples Based on Indirect Competitive ELISA Method Using Iron-Cobalt Co-Doped Carbon Dots Labeled Histamine Antibody. *Food Chem.* **2021**, *345*, 128812. <https://doi.org/10.1016/j.foodchem.2020.128812>.
- (22) Luo, L.; Wei, X.-Q.; Jia, B.-Z.; Yang, J.-Y.; Shen, Y.-D.; Hammock, B.; Dong, J.-X.; Wang, H.; Lei, H.-T.; Xu, Z.-L. Modulating Linker Composition of Haptens Resulted in Improved Immunoassay for Histamine. *Biomolecules* **2019**, *9* (10), 597. <https://doi.org/10.3390/biom9100597>.
- (23) Xiao, X.; Li, H.; Zhao, L.; Zhang, Y.; Liu, Z. Oligonucleotide Aptamers: Recent Advances in Their Screening, Molecular Conformation and Therapeutic Applications. *Biomed. Pharmacother.* **2021**, *143*, 112232. <https://doi.org/10.1016/j.biopha.2021.112232>.
- (24) Dwidar, M.; Seike, Y.; Kobori, S.; Whitaker, C.; Matsuura, T.; Yokobayashi, Y. Programmable Artificial Cells Using Histamine-Responsive Synthetic Riboswitch. *J. Am. Chem. Soc.* **2019**, *141* (28), 11103–11114. <https://doi.org/10.1021/jacs.9b03300>.
- (25) John Ho, L. S.; Fogel, R.; Limson, J. L. Generation and Screening of Histamine-Specific Aptamers for Application in a Novel Impedimetric Aptamer-Based Sensor. *Talanta* **2020**, *208*, 120474. <https://doi.org/10.1016/j.talanta.2019.120474>.
- (26) Mairal Lerga, T.; Jauset-Rubio, M.; Skouridou, V.; Bashammakh, A. S.; El-Shahawi, M. S.; Alyoubi, A. O.; O'Sullivan, C. K. High Affinity Aptamer for the Detection of the Biogenic Amine Histamine. *Anal. Chem.* **2019**, *91* (11), 7104–7111. <https://doi.org/10.1021/acs.analchem.9b00075>.
- (27) Mairal Lerga, T.; Skouridou, V.; Bermudo, M. C.; Bashammakh, A. S.; El-Shahawi, M. S.; Alyoubi, A. O.; O'Sullivan, C. K. Gold Nanoparticle Aptamer Assay for the Determination of Histamine in Foodstuffs. *Microchim. Acta* **2020**, *187* (8), 452. <https://doi.org/10.1007/s00604-020-04414-4>.
- (28) Dwidar, M.; Yokobayashi, Y. Development of a Histamine Aptasensor for Food Safety Monitoring. *Sci. Rep.* **2019**, *9* (1), 16659. <https://doi.org/10.1038/s41598-019-52876-1>.

- (29) *FRET - Förster Resonance Energy Transfer: From Theory to Applications*; Medintz, I. L., Hildebrandt, N., Eds.; John Wiley & Sons, 2013.
- (30) Algar, W. R.; Hildebrandt, N.; Vogel, S. S.; Medintz, I. L. FRET as a Biomolecular Research Tool — Understanding Its Potential While Avoiding Pitfalls. *Nat. Methods* **2019**, *16* (9), 815–829. <https://doi.org/10.1038/s41592-019-0530-8>.
- (31) Chen, J.; Shi, C.; Kang, X. yue; Shen, X. tong; Lao, X.; Zheng, H. Recent Advances in Fluorescence Resonance Energy Transfer-Based Probes in Nucleic Acid Diagnosis. *Anal. Methods* **2020**, *12* (7), 884–893. <https://doi.org/10.1039/C9AY02332A>.
- (32) Qiu, X.; Hildebrandt, N. A Clinical Role for Förster Resonance Energy Transfer in Molecular Diagnostics of Disease. *Expert Rev. Mol. Diagn.* **2019**, *19* (9), 767–771. <https://doi.org/10.1080/14737159.2019.1649144>.
- (33) *The Immunoassay Handbook*, 4th ed.; Wild, D., Ed.; Elsevier, 2013.
- (34) Zwier, J. M.; Hildebrandt, N. Time-Gated FRET Detection for Multiplexed Biosensing. In *Reviews in Fluorescence 2016*; Geddes, CD, Ed.; Reviews in Fluorescence; Springer, Cham, 2017; pp 17–43. [https://doi.org/10.1007/978-3-319-48260-6\\_3](https://doi.org/10.1007/978-3-319-48260-6_3).
- (35) Qiu, X.; Xu, J.; Cardoso Dos Santos, M.; Hildebrandt, N. Multiplexed Biosensing and Bioimaging Using Lanthanide-Based Time-Gated FRET. *Acc. Chem. Res.* **2022**, *55* (4), 551–564. <https://doi.org/10.1021/acs.accounts.1c00691>.
- (36) Sy, M.; Nonat, A.; Hildebrandt, N.; Charbonniere, L. J. Lanthanide-Based Luminescence Biolabelling. *Chem. Commun.* **2016**, *52* (29), 5080–5095. <https://doi.org/10.1039/c6cc00922k>.
- (37) Xu, J.; Guo, J.; Golob-Schwarzl, N.; Haybaeck, J.; Qiu, X.; Hildebrandt, N. Single-Measurement Multiplexed Quantification of MicroRNAs from Human Tissue Using Catalytic Hairpin Assembly and Förster Resonance Energy Transfer. *ACS Sens.* **2020**, *5* (6), 1768–1776. <https://doi.org/10.1021/acssensors.0c00432>.
- (38) Dekaliuk, M.; Qiu, X.; Troalen, F.; Busson, P.; Hildebrandt, N. Discrimination of the V600E Mutation in BRAF by Rolling Circle Amplification and Förster Resonance Energy Transfer. *ACS Sens.* **2019**, *4* (10), 2786–2793. <https://doi.org/10.1021/acssensors.9b01420>.
- (39) Qiu, X.; Xu, J.; Guo, J.; Yahia-Ammar, A.; Kapetanakis, N.-I.; Duroux-Richard, I.; Unterluggauer, J. J.; Golob-Schwarzl, N.; Regard, C.; Uzan, C.; Gouy, S.; DuBow, M.; Haybaeck, J.; Apparailly, F.; Busson, P.; Hildebrandt, N. Advanced MicroRNA-Based Cancer Diagnostics Using Amplified Time-Gated FRET. *Chem. Sci.* **2018**, *9* (42), 8046–8055. <https://doi.org/10.1039/c8sc03121e>.
- (40) Qiu, X.; Wegner, K. D.; Wu, Y.-T.; Henegouwen, P. M. P. van B. en; Jennings, T. L.; Hildebrandt, N. Nanobodies and Antibodies for Duplexed EGFR/HER2 Immunoassays Using Terbium-to-Quantum Dot FRET. *Chem. Mater.* **2016**, *28* (22), 8256–8267. <https://doi.org/10.1021/acs.chemmater.6b03198>.
- (41) Geißler, D.; Stufler, S.; Löhmannsröben, H.-G.; Hildebrandt, N. Six-Color Time-Resolved Förster Resonance Energy Transfer for Ultrasensitive Multiplexed Biosensing. *J. Am. Chem. Soc.* **2013**, *135* (3), 1102–1109. <https://doi.org/10.1021/ja310317n>.

- (42) Hildebrandt, N. How to Apply FRET: From Experimental Design to Data Analysis. In *FRET – Förster Resonance Energy Transfer*; Medintz, I. L., Hildebrandt, N., Eds.; Wiley-VCH Verlag GmbH & Co. KGaA, Weinheim, 2013; pp 105–163. <https://doi.org/10.1002/9783527656028.ch05>.
- (43) Hildebrandt, N.; Wegner, K. D.; Algar, W. R. Luminescent Terbium Complexes: Superior Förster Resonance Energy Transfer Donors for Flexible and Sensitive Multiplexed Biosensing. *Coord. Chem. Rev.* **2014**, *273–274*, 125–138. <https://doi.org/10.1016/j.ccr.2014.01.020>.
- (44) Lehane, L.; Olley, J. Histamine Fish Poisoning Revisited. *Int. J. Food Microbiol.* **2000**, *58* (1), 1–37. [https://doi.org/10.1016/S0168-1605\(00\)00296-8](https://doi.org/10.1016/S0168-1605(00)00296-8).
- (45) Tao, Z.; Sato, M.; Zhang, H.; Yamaguchi, T.; Nakano, T. A Survey of Histamine Content in Seafood Sold in Markets of Nine Countries. *Food Control* **2011**, *22* (3), 430–432. <https://doi.org/10.1016/j.foodcont.2010.09.018>.
- (46) Ordóñez, J. L.; Callejón, R. M.; Troncoso, A. M.; García-Parrilla, M. C. Evaluation of Biogenic Amines Profile in Opened Wine Bottles: Effect of Storage Conditions. *J. Food Compos. Anal.* **2017**, *63*, 139–147. <https://doi.org/10.1016/j.jfca.2017.07.042>.
- (47) Esposito, F.; Montuori, P.; Schettino, M.; Velotto, S.; Stasi, T.; Romano, R.; Cirillo, T. Level of Biogenic Amines in Red and White Wines, Dietary Exposure, and Histamine-Mediated Symptoms upon Wine Ingestion. *Molecules* **2019**, *24* (19), 3629. <https://doi.org/10.3390/molecules24193629>.
- (48) Chen, C.; Corry, B.; Huang, L.; Hildebrandt, N. FRET-Modulated Multihybrid Nanoparticles for Brightness-Equalized Single-Wavelength Barcoding. *J. Am. Chem. Soc.* **2019**, *141* (28), 11123–11141. <https://doi.org/10.1021/jacs.9b03383>.
- (49) West, W.; Geddes, A. L. The Effects of Solvents and of Solid Substrates on the Visible Molecular Absorption Spectrum of Cyanine Dyes. *J. Phys. Chem.* **1964**, *68* (4), 837–847. <https://doi.org/10.1021/j100786a023>.
- (50) Levitus, M.; Ranjit, S. Cyanine Dyes in Biophysical Research: The Photophysics of Polymethine Fluorescent Dyes in Biomolecular Environments. *Q. Rev. Biophys.* **2011**, *44* (1), 123–151. <https://doi.org/10.1017/S0033583510000247>.
- (51) Guddat, L. W.; Herron, J. N.; Edmundson, A. B. Three-Dimensional Structure of a Human Immunoglobulin with a Hinge Deletion. *Proc. Natl. Acad. Sci. USA* **1993**, *90* (9), 4271–4275. <https://doi.org/10.1073/pnas.90.9.4271>.
- (52) Stein, P. E.; Leslie, A. G. W.; Finch, J. T.; Carrell, R. W. Crystal Structure of Uncleaved Ovalbumin at 1.95 Å Resolution. *J. Mol. Biol.* **1991**, *221* (3), 941–959. [https://doi.org/10.1016/0022-2836\(91\)80185-W](https://doi.org/10.1016/0022-2836(91)80185-W).
- (53) Guo, J.; Qiu, X.; Mingoos, C.; Deschamps, J. R.; Susumu, K.; Medintz, I. L.; Hildebrandt, N. Conformational Details of Quantum Dot-DNA Resolved by Förster Resonance Energy Transfer Lifetime Nanoruler. *ACS Nano* **2019**, *13* (1), 505–514. <https://doi.org/10.1021/acsnano.8b07137>.
- (54) Léger, C.; Yahia-Ammar, A.; Susumu, K.; Medintz, I. L.; Urvoas, A.; Valerio-Lepiniec, M.; Minard, P.; Hildebrandt, N. Picomolar Biosensing and Conformational Analysis Using Artificial Bidomain Proteins and Terbium-to-Quantum Dot Förster Resonance Energy Transfer. *ACS Nano* **2020**, *14* (5), 5956–5967. <https://doi.org/10.1021/acsnano.0c01410>.

- (55) Zhang, B.; Sheng, W.; Liu, Y.; Huang, N.; Zhang, W.; Wang, S. Multiplexed Fluorescence Immunoassay Combined with Magnetic Separation Using Upconversion Nanoparticles as Multicolor Labels for the Simultaneous Detection of Tyramine and Histamine in Food Samples. *Anal. Chim. Acta* **2020**, *1130*, 117–125. <https://doi.org/10.1016/j.aca.2020.07.043>.
- (56) Lerga, T. M.; Skouridou, V.; Bermudo, M. C.; Bashammakh, A. S.; El-Shahawi, M. S.; Alyoubi, A. O.; O’Sullivan, C. K. Gold Nanoparticle Aptamer Assay for the Determination of Histamine in Foodstuffs. *Microchim. Acta* **2020**, *187* (8), 452. <https://doi.org/10.1007/s00604-020-04414-4>.

